ADVANCED MATERIALS INTERFACES

www.advmatinterfaces.de

The Facet Structure and Photochemical Reactivity of Arbitrarily Oriented Strontium Titanate Surfaces

*Ajay S. Pisat, Paul A. Salvador, and Gregory S. Rohrer**

$SrTiO_3$ polycrystalline ceramics with polished surfaces are annealed at 1250 °C in air. This treatment causes the flat surfaces to break up into facets meeting at sharp edges and corners. An analysis of the orientations and topography of the faceted surfaces demonstrates that all are either {100} or {110} oriented. The {100} surfaces are photocathodically active and reduce Ag^+ to Ag metal. The {110} surfaces are photoanodically active and oxidize Mn^{2+} and Pb^{2+} to Mn^{4+} and Pb^{4+}, respectively. The chemical properties of both surfaces appear to be uniformly photocathodic or photoanodic. However, after annealing at 1100 °C with $Sr_3Ti_2O_7$, the {110} facets have a combination of photocathodic and photoanodic terraces. The results show that the photocathodic-to-photoanodic surface area ratio, which influences the overall rate of a photochemical reaction, can be controlled for arbitrarily oriented $SrTiO_3$ surfaces by using thermal treatments to create low index facets and to control the chemical terminations on these facets.

1. Introduction

Photocatalysis is the process of using light to increase the rate of a chemical reaction. This phenomenon has tremendous potential in applications such as water splitting[1] and the purification of water[2] and air.[3] However, the efficiencies of photocatalytic processes are low, especially when sunlight is used to drive them.[4] Separating photogenerated electron–hole pairs in photocatalysts is an absolute necessity for efficient photocatalysis.[5] One way of achieving this is by engineering spatial selectivity into the material. Spatial selectivity means that the photoanodic reaction sites are spatially separated and distinct from the photocathodic reaction sites. Simulations have suggested that it might be possible to optimize a ferroelectric photocatalytic material with spatially selective photocathodic and photoanodic domains to minimize internal recombination and thus improve efficiency from less than 1% to over 90% of the theoretical maximum.[6,7] Because efficiency is the factor most limiting the commercialization of climate-change fighting concepts such as solar water splitting, it is important to study and understand the spatial selectivity of reactivity of the surfaces of photocatalysts.

A. S. Pisat, Prof. P. A. Salvador, Prof. G. S. Rohrer
Carnegie Mellon University
3325 Wean Hall, 5000 Forbes Avenue, PA 15213, USA
E-mail: gr20@andrew.cmu.edu

The ORCID identification number(s) for the author(s) of this article can be found under https://doi.org/10.1002/admi.201900731.

DOI: 10.1002/admi.201900731

Spatial selectivity of reaction sites is made possible by having an electrochemical potential difference between distinct regions on a given surface.[5] Noble metal co-catalysts are very commonly added to photocatalysts to engender spatial selectivity and achieve some empirically optimized balance between reactions on the distinct surfaces.[8–10] For some materials, however, spatial selectivity can be attained without the addition of another phase. Bai et al.[11] and Li et al.[12] reviewed mechanisms that lead to charged surface domains that promote charge separation. Spatially distinct photoanodic and photocathodic domains may arise from different polarities of ferroelectric domains,[13–17] different surface electronic energy levels of distinct crystalline facets (surface orientation),[18–20] different surface polarities of ferroelastic domains,[21–24] and different chemical terminations on a single orientation.[25–27] All of these mechanisms for creating charged surface domains have been investigated individually. However, for catalysts that expose multiple surfaces, which is the case for most particles and polycrystals, charged surface domains might arise from more than one mechanism. For example, if the catalyst exposes multiple surface orientations to the reaction environment, and one or more of these surfaces has differently charged surface domains because of multiple chemical terminations, then chemical potential differences can arise because of both the surface orientation and the surface termination. In cases where the material is ferroelectric or ferroelastic, there are additional sources of chemical potential differences. Because we do not currently understand the relative importance of charged surface domains created by these different mechanisms, it is important to study their effect on chemical reactivity when they co-exist on the same catalyst.

Here, we study arbitrarily oriented surfaces of cubic perovskite structured $SrTiO_3$. This material is interesting because Al-doped $SrTiO_3$, activated with a $Rh_{2-y}CryO_3$ catalyst, has been shown to split water in sunlight.[28] There are two mechanisms that can create charged surface domains on $SrTiO_3$. The first is that differently oriented surfaces are relatively more photocathodic or photoanodic.[29,30] At 1250 °C, $SrTiO_3$ surfaces are mostly made up of {100} and {110} facets and, at higher temperatures, {111} facets also appear on the equilibrium crystal shape,[31,32] and each of these surfaces has a different photochemical reactivity.[17] The second mechanism that can create charged surface domains is that $SrTiO_3$ surfaces can have different chemical terminations, with different charges, that

 © 2019 WILEY-VCH Verlag GmbH & Co. KGaA, Weinheim

promote the photocathodic and photoanodic half reactions differently.[33] For example, the two possible chemical terminations of the $SrTiO_3$ (100) surface are SrO or TiO_2, and the two possible chemical terminations of the $SrTiO_3$ (110) are O_2^{4-} and $SrTiO^{4+}$. It should be emphasized that here we refer to the ideal terminations when the crystal is cleaved and the atomic positions do not significantly change. In reality, the surface is likely to reconstruct and this will depend on the external environment,[34,35] but such changes do not completely eliminate the surface charge.

Small, polygonal $SrTiO_3$ crystals have been shown to have orientation dependent photochemical reactivity that depends on crystal shape.[29,30] When the crystals were terminated only by {100} planes, the {100} facets were both photocathodic and photoanodic. However, when the crystals were engineered to have {100} and {110} facets, the {100} surfaces were relatively photocathodic and the {110} surface were relatively photoanodic.[29,30] Giocondi and Rohrer[33] showed that single crystal $SrTiO_3$(110) and (111) surfaces can simultaneously support relatively photoanodic and photocathodic terraces with different chemical terminations, and Zhu et al.[26,27] showed that it was possible to adjust the relative areas of these terraces. By exposing $SrTiO_3$ single crystals to Sr-rich and Sr-deficient atmospheres at high temperatures, the surfaces were made Sr-rich or deficient, respectively (likely by vapor transport of $Sr(OH)_2$). By controlling the time and temperature of annealing in various conditions, the photocathodic area fraction of the (111) surface could be changed from 14% to 55%.[26] Similarly, the photocathodic area fraction of the (110) surface could be changed from 0% to 98%.[27] These results indicate that, by controlling the particle shape and chemical termination, it is possible to control the relative areas of photocathodic and photoanodic areas on the $SrTiO_3$ surface. Furthermore, it was recently demonstrated that surface terminations can also influence thermocatalytic reactions; Polo-Garzon et al.[25] used thermochemical treatments to control the surface terminations of $SrTiO_3$ powders and showed that this influenced the selectivity for the conversion of 2-propanol to propene and acetone.

The purpose of this paper is to show that the photochemical reactivity of arbitrarily oriented $SrTiO_3$ surfaces can be tuned in a manner similar to the low index orientations of single crystal $SrTiO_3$. While one might expect a low index facet on an arbitrarily oriented surface to behave in the same way as a single crystal with that low index orientation, there is an important difference. For the case of a single crystal with a near atomically flat surface, both the reduction and oxidation half reactions have to occur on the same surface. For the case of an arbitrarily oriented crystal whose equilibrium crystal shape is made up of a limited number of facets, surfaces exposed to high temperature annealing will be constructed of facets with multiple orientations, and the reduction reaction can occur on the more photocathodic orientation and the oxidation reaction on the more photoanodic orientation. The role of charged surface domains in this case is not clear. Therefore, thermochemical treatments inspired by reference[27] were used to alter the relative areas of photocathodic and photoanodic terraces on thermally induced low index facets on $SrTiO_3$ and the influence of this on the photochemical reactions was determined. What is new about the current experiments is that samples are used that simultaneously have different relative areas of different surface orientations and different charged domains with different chemical terminations. This situation makes it possible to explore the simultaneous influence of multiple surface orientations and different charged domains on the spatial selectivity of photodeposition reactions. The results show that both surface orientation and the charged domains are influential in determining the photochemical reactivity.

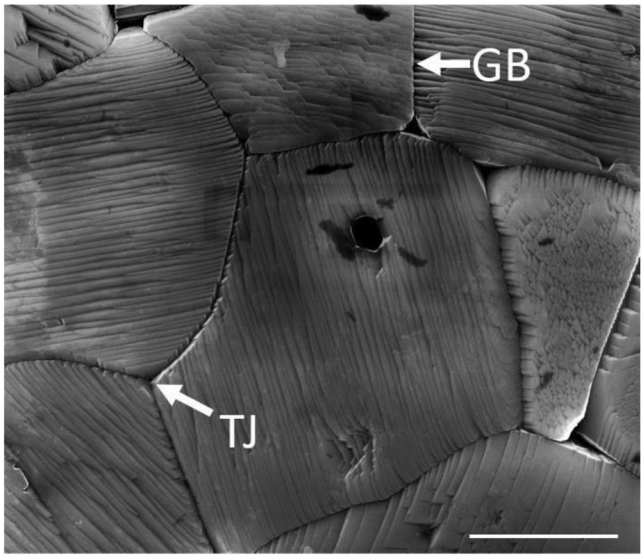

Figure 1. Secondary electron image of the $SrTiO_3$ sample surface after the baseline thermal treatment. The scale bar is 3 μm.

2. Results

The surface of the $SrTiO_3$ crystal after the baseline thermal treatment is shown in **Figure 1**. A grain boundary and a triple junction are labeled GB and TJ, respectively. The contrast within the grains results from sets of facets that replaced the original, flat, polished surface. While the facets increase the surface area, they lower the total surface energy by replacing the original surface with lower energy surfaces.[36]

The surface orientations of the facets on seven grains were determined using topographic atomic force microscopy (AFM) data, electron backscatter diffraction (EBSD) crystal orientation data, and the procedure described in the Experimental Section. An example of a 3D representation of the topographic AFM data from a faceted surface is shown in **Figure 2**a. Two directions normal to the surface are illustrated by the white arrows. For seven different grains, 750 surface normals were extracted and they are shown in the crystal reference frame in Figure 2b. The orientations are plotted in the standard stereographic triangle, which represents all distinguishable surface orientations in the cubic system. The surface normals are strongly clustered about the (001) and (101) orientations. Deviations from the ideal (001) and (101) orientations are most likely the result of uncertainties in the surface normal measurement; because of the finite curvature of the AFM tip, the sharp facet intersections are rounded so that locally, there is a more continuous range

© 2019 WILEY-VCH Verlag GmbH & Co. KGaA, Weinheim

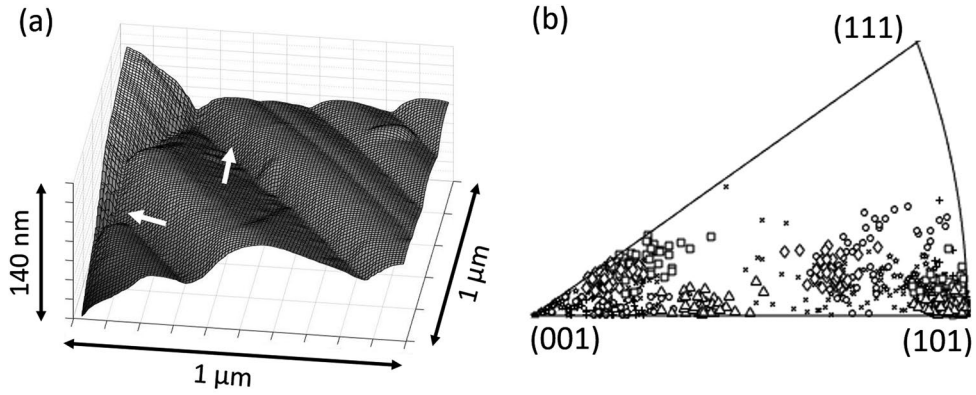

Figure 2. a) A 3D representation of the topographic AFM data; two surface normals are indicated by the white arrows. b) The orientations of 750 surface normals from seven grains projected onto the standard stereographic triangle. A different symbol is used for the normals from different grains.

of orientations. It is also possible that a finite and continuous range of vicinal orientations are permitted near the ideal low index orientations, as reported for samples annealed at higher temperature.[32] In either case, we interpret the result to mean that the faceted $SrTiO_3$ surfaces that result from annealing at 1250 °C are constructed of {100} and {110} surfaces, and possibly some orientations vicinal to these surfaces. We note that this interpretation is consistent with the data reported by Rheinheimer et al.,[31] who concluded that the equilibrium crystal shape at this temperature consists of {100} and {110} facets.

The photochemical reactivity of the faceted surfaces suggests that the two different facets have distinctly different reactivities. For example, the secondary electron (SE) images in **Figure 3** show the surface after the photochemical reduction of Ag^+; this is a surface that was subjected to the baseline treatment. The silver appears as small particles with white contrast in Figure 3a,b. In Figure 3a, at least one set of facets in all grains is decorated with reaction product (white contrast). Conversely, at least one set of facets on each grain has almost no observable reduced silver. The selectivity of the silver reduction shows that one of the two orientations is strongly photocathodic while the other is not. The same phenomenon was observed for all grains. A higher magnification image of the surface of a single grain is shown in Figure 3b. False color has been added in a region of Figure 3b to demarcate photocathodic (blue) and non-photocathodic (pink) sets of facets. For added clarity, this is represented schematically in Figure 3c. The schematic illustrates the hill-and-valley structure formed by the facets, with only the blue-colored facets active for silver reduction.

To determine the orientations of photocathodic (photoanodic) facets, the surfaces were used to photoreduce (photooxidize) Ag^+ (Mn^{2+}). The SE images in **Figure 4**a,d show grains after a 6 s photoreduction reaction and a 1 min photooxidation reaction, respectively. The particles with white contrast in Figure 4a are photodeposited silver. The filamentary, web-like deposit in Figure 4d is MnO_x. 3D representations of the areas enclosed in red squares in Figure 4a,d are illustrated in Figure 4b,e, respectively. The reactive facets in both instances have been labeled and colored (blue/pink) to make it easy to identify the facet reactivity (cathodic/anodic). As mentioned before, it is assumed that the facets meet at a sharp edge, but the intersection appears rounded because of the finite curvature of the AFM tip. The surface normal vectors, obtained from the AFM data and transformed into the crystal reference frame using the grain orientation data, are plotted on a standard stereographic triangle in Figure 4c,f for the photocathodic and photoanodic

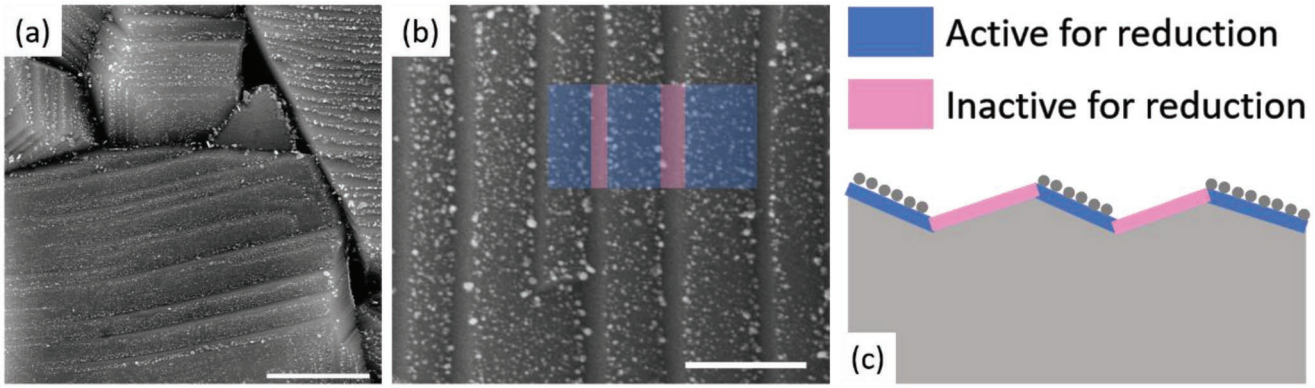

Figure 3. a) SEM image of a surface after the photoreduction of Ag^+. The scale bar is 2 µm. b) Zoomed-in image of a single grain surface made up of two facets, where one is active for photoreduction and the other is not. The scale bar is 1 µm. c) Schematic of the hill-and-valley topography of the facets. The blue-colored facets are photocathodic and correspond to the area in (b) marked with the same color, and the grey circles represent photoreduced silver.

© 2019 WILEY-VCH Verlag GmbH & Co. KGaA, Weinheim

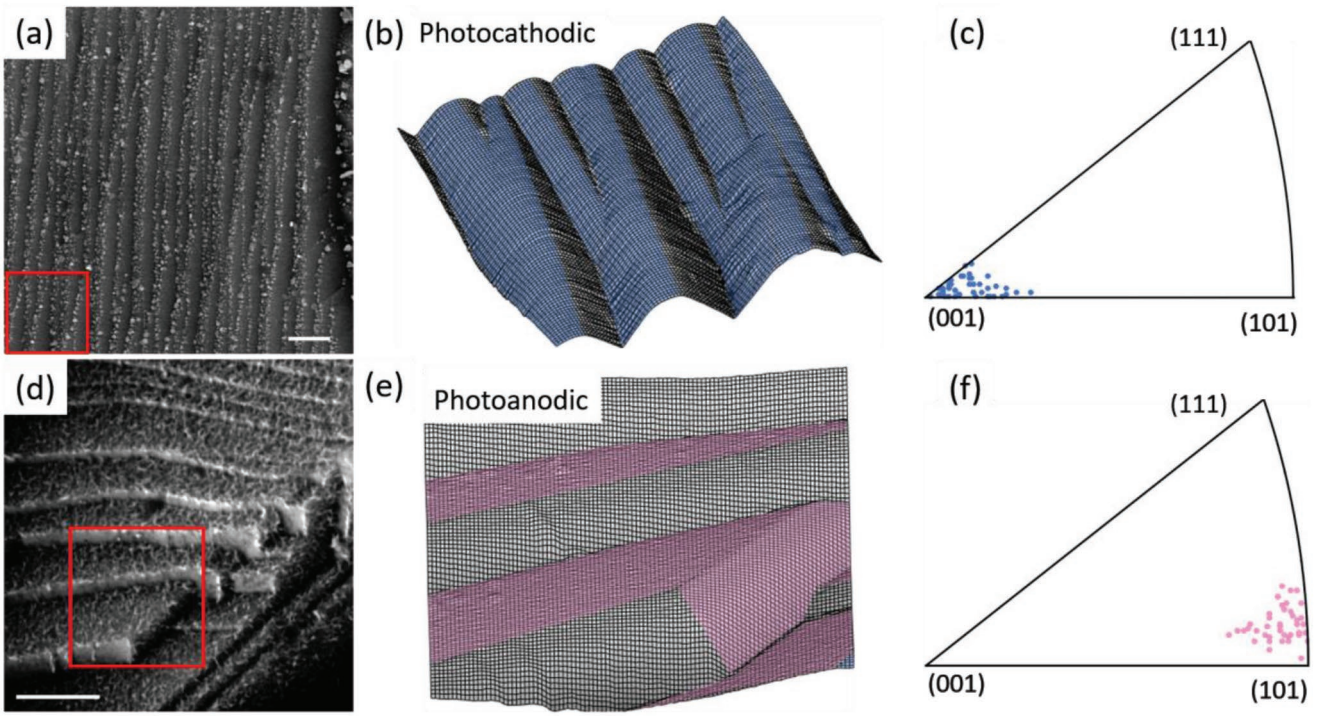

Figure 4. a) SE image of a grain after photoreduction. b) 3D representation of an AFM image from the area in (a) denoted by the red square. c) Standard stereographic projection showing the orientations of 50 surface normals in the crystal reference frame from (b). d) SE image of a grain after photooxidation. In (a,d) the scale bar is 500 nm. e) 3D representation of an AFM image from the area in (d) denoted by the red square. f) Standard stereographic projection showing the orientations of 50 surface normals in the crystal reference frame from (e). Vertical scales: b) 330 nm e) 55 nm.

reaction, respectively. Each orientation distribution contains 50 randomly selected points from the photocathodic and photoanodic facet surfaces shown in Figure 4b,e, respectively. The results in Figure 4c,f clearly show that the photocathodic facets have near {100} orientations and the photoanodic facets have near {110} orientations. This conclusion was reached from all areas examined. In cases where three facets were observed, two of the three promoted either reduction or oxidation and were found to be in the {100} or the {110} family, respectively. Again, the scatter in the measured orientations is attributed to the curvature introduced by the shape of the AFM tip.

To confirm that different sets of facets carry out different reactions on a single grain, we examined by the photoreduction of silver and the photooxidation of manganese on the same grain. The AFM images in **Figure 5**a–c show the topography of the same area of one $SrTiO_3$ grain before any reaction, after photoreduction, and after photooxidation, respectively. There are two sets of facets on this grain. Comparing Figure 5a (before reaction) with Figure 5b (after photoreduction), one of these sets of facets is covered with higher (white contrast) features that result from the photoreduction of Ag^+. Therefore, these are the photocathodic facets. When one compares Figure 5a (before reaction) with Figure 5c (after photooxidation), the other set of facets is covered with higher (white contrast) features that result from the photooxidation of Mn^{2+}. Therefore, these are the photoanodic facets. To illustrate the distinct characteristics of these facets, Figure 5d shows a 3D representation of the area in the black outline from Figure 5a, where the photocathodic

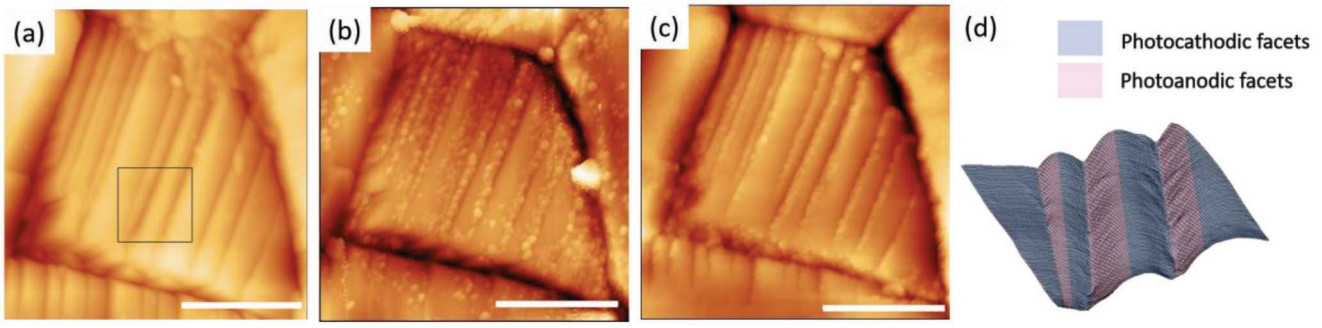

Figure 5. AFM topography of a grain (a) before reaction, b) after photoreduction and c) after photooxidation. d) 3D representation of area inside black box in (a) colored by reactivity. The scale bar is 1 µm. Vertical scales (dark to bright): a) 210 nm, b) 162 nm, c) 187 nm.

© 2019 WILEY-VCH Verlag GmbH & Co. KGaA, Weinheim

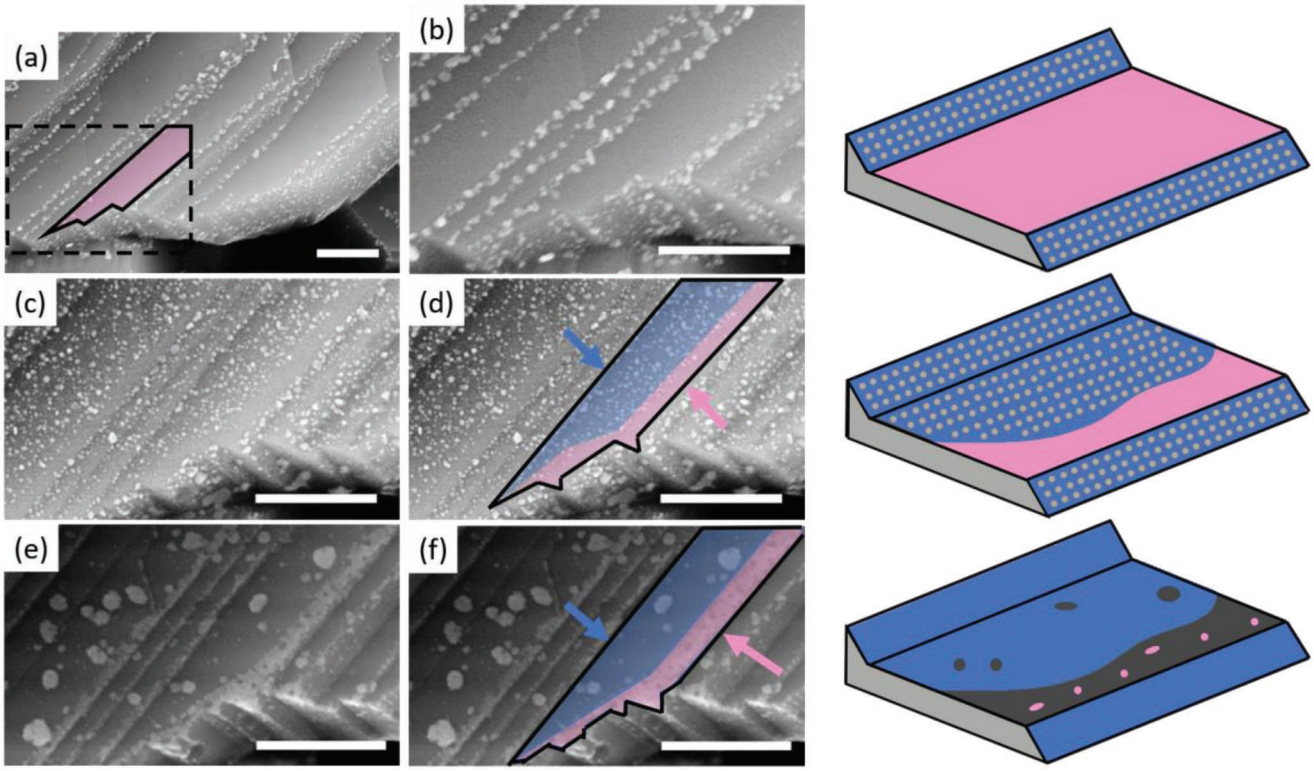

Figure 6. SEM images of the same area of $SrTiO_3$ grain after different treatments. a) Large field of view image showing large (110) terraces after the reduction of silver. b) View of the area of interest. c) After a thermal treatment (5 h/1100 °C/0.1 g $Sr_3Ti_2O_7$) to make the surface Sr-rich, silver is reduced on more of the surface, including area with the (110) orientation. d) False color has been added to (c) to highlight areas with silver (blue) and areas without silver (pink). e) The same surface after the oxidation of lead. f) False color has been added to (e) to highlight areas covered by oxidized lead (pink) and those with less lead (blue). In the schematics, photocathodic areas are blue, photoanodic areas are pink, silver particles are light grey, and lead deposits are dark grey. In all images, the scale bar is 500 nm.

(photoanodic) facets have been colored blue (pink). The finding from these observations is that reduction and oxidation take place on complementary sets of facets on the same grain in the baseline samples. This is observed consistently for all grains.

Finally, the photochemical reactivity of a surface was studied before and after a thermochemical treatment in an environment with a Sr-excess to determine if the surface reactivity could be changed. The SEM images in **Figure 6** show a grain whose large, flat terraces have the {110} orientation. Figure 6a shows the surface after photoreduction of silver. There is almost no reduced silver on the {110} facets. Instead, silver particles with white contrast decorate only the {100}-oriented ledges. For the images in Figure 6b–f, we focus only on the area within the black, dashed, rectangle and the photocathodically inert terrace that is colored pink. This region is shown, with no markings, in Figure 6b, and the terrace is illustrated schematically to the right.

After being used to reduce silver, the surface was cleaned and heated for 5 h at 1100 °C with 0.1 g of $Sr_3Ti_2O_7$. Following Zhu et al.,[26,27] this thermal treatment makes the surfaces relatively Sr-rich. When silver is photochemically reduced on the thermally treated surface (15 s exposure), in addition to {100} ledges, reduced silver is found on a greater fraction of the {110} flat terraces (see Figure 6c) than after the baseline treatment (see Figure 6b). Some areas appear to be free of silver particles and for clarity, one of them is marked by pink in Figure 6d. The sample was then cleaned and subjected to photooxidation of lead (16 s exposure). As shown in Figure 6e, the areas that reduced the most silver now have a few larger lead deposits, while the areas that did not reduce silver are coated with oxidized lead. The areas coated with oxidized lead are highlighted in pink in Figure 6f, and the oxidized lead is shown as dark gray in the schematic, with the pink photoanodic surface visible between breaks in the oxidized lead coating. Because the thermal treatment increased the relative area of the surface that reduces silver, it is more photocathodic. Note that while the {110} surface was originally photoanodic after the baseline treatment, it becomes bifunctional after the treatment in excess Sr, with part of the surface being photocathodic. This change is illustrated by the schematics on the right side of Figure 6 (and is consistent with observations made for single crystals[27]).

3. Discussion

The photochemical reactivity of arbitrarily oriented crystals at the surface of a $SrTiO_3$ polycrystal can be interpreted in a surprisingly simple way. Because a general crystal orientation {*hkl*} of $SrTiO_3$ always breaks up into a combination of {100} and {110} facets under the annealing conditions used, the reactivity of the surface is simply a combination of the reactivity of

© 2019 WILEY-VCH Verlag GmbH & Co. KGaA, Weinheim

the {100} and {110} orientations. The relative areas of the {100} and {110} facets vary with the macroscopic crystal orientation, {*hkl*}.[37] The results show that the {110} oriented facets are more photoanodic and the {100} facets are more photocathodic. This suggests that it is possible to transfer photogenerated electrons to the more photocathodic orientation and photogenerated holes to the more photoanodic orientation. The result is that when a high index surface orientation breaks up into {100} and {110} facets, these two orientations provide an abundance of photocathodic and photoanodic sites to promote the overall reaction.

For an ideally orientated single crystal surface (nearly atomically flat), the situation is different. In this case, if there are no steps, the oxidation and reduction reactions must occur on the same surface. For $SrTiO_3$, the photocathodic and photoanodic reactions can be supported by differently charged surface domains that arise from differences in the chemical terminations.[33] However, the results presented here suggest that differently charged surface domains are not apparent, nor are they necessary, when {100} and {110} facets are simultaneously present on surfaces annealed in standard conditions (1250 °C, 8 h, in air). This is consistent with the findings of Mu et al.,[30] who studied the photochemical reactivity of sub-micrometer, polygonal $SrTiO_3$ crystals. They found that cube-shaped crystals terminated by only {100} surfaces supported both photocathodic and photoanodic reactions. However, when crystals had both {100} and {110} facets, the photocathodic reaction occurred exclusively on {100} and the photoanodic reaction occurred exclusively on {110}. From this, one can conclude that the photoanodic sites on the {110} surface are more favorable than any such sites on the {100} surface.

One of the questions motivating this study was to understand the relative importance of surface termination (the chemical composition of the surface) versus the surface orientation. Information from the earlier single crystal studies can be used to identify the most likely terminations after the baseline thermal treatment (1250 °C, 8 h, in air). Zhu et al.[27] reported that after heating a (110) orientated $SrTiO_3$ single crystal at 1200 °C for 12 h, 90% of the surface area is photoanodic and after 24 h it was 100% photoanodic. Although our baseline treatment was for only 8 h, is was at a higher temperature, so it is safe to assume that the surface is also mostly, if not entirely, photoanodic. In fact, the results show that {110} surfaces are almost completely photoanodic, with only negligible amounts of silver reduced on these surfaces. The other principal facet is {100}. Although the chemical properties of this surface have not been reported, details of the surface structure after similar thermal treatments have been reported. Bachelet et al.[38] reported that after heating a (100) orientated $SrTiO_3$ single crystal at 1300 °C for 8 h, the surface had a roughly equal mix of SrO and TiO_2 terminated surfaces. Considering the similarity of our annealing conditions, it is reasonable to assume that the surfaces in the present study had a similar composition. Ocal et al.[39] reported that the measured surface potential difference between the SrO and TiO_2 terminations on a (100) oriented single crystal is ≈45 mV. On the $SrTiO_3$ (110) surface, potential differences as small at 10 mV[27] led to the spatial separation of reaction products, so it seems likely that the same thing should occur {100} surfaces, but this was not observed. This is probably because of the simultaneous presence of {110} facets. As noted above, the {110} surface appears to be more anodic than any sites on the {100} surface, so that the photocathodic reaction occurs exclusively on the {100} surface and the photoanodic reaction occurs exclusively on the {110} surface.

If one considered only the experiments after the baseline thermal treatment, where there is no evidence that charged surface domains from termination differences influence the reactivity, it would be concluded that the surface orientation is more important than the chemical termination. However, the observations after the thermal treatment with $Sr_3Ti_2O_7$ shows that this does not have to be the case. According to Zhu et al.,[27] annealing in the presence of $Sr_3Ti_2O_7$ should increase the relative area of photocathodic domains on the {110} surface. This is confirmed in Figure 6, which shows that parts of the {110} terraces become photocathodic (and less photoanodic) after the heat treatment. In previous work,[26] photocathodic behavior was associated with a surface composition that had a greater Sr/Ti ratio, and this is consistent with the expected result of heating the surface in the presence of $Sr_3Ti_2O_7$. It is currently not known what effect the heat treatment might have on the surface terminations of the {100} surface. However, the treatment promotes photocathodic reactivity and it is therefore not surprising that the originally photocathodic {100} surface remains photocathodic after the thermal treatment.

The relative areas of photocathodic and photoanodic surfaces on a catalyst particle are important for the overall reactivity. The schematic crystal shown in **Figure 7**a can simultaneously promote oxidation and reduction, which is necessary for the photochemical reaction to proceed. In this case, the 6 {100} surfaces promote the photocathodic reaction and the 12 {110} surfaces promote the photoanodic reaction. It is assumed that electrons and holes generated in the bulk can migrate to the appropriate surface. This is supported by simulations that showed that small differences in surface potential cause electrons and holes to migrate to oppositely charged surfaces with little recombination.[6,7] However, for the reaction to proceed at the maximum rate, the oxidation and reduction must proceed at their maximum equal rates. One way to manipulate the relative reaction rates it to control the photocathodic to photoanodic surface area ratio. This could be accomplished by changing the shape of the crystal (the relative areas of {100} and {110} surface). Another possibility is to use thermochemical treatments, as demonstrated here, that create photocathodic surface domains on the {110} surfaces. For example, Figure 7b schematically illustrates how photocathodic-to-photoanodic surface area ratio of the particle in Figure 7a could be increased by annealing in a Sr-rich environment.

4. Conclusions

The surfaces of $SrTiO_3$ crystals with arbitrary orientations, after heating in air at 1250 °C for 8 h, are terminated by a combination of {110} and {100} facets and the relative areas of the two facets depends on the orientation, {*hkl*}. The {100} facets appear to be uniformly photocathodic and serve as reduction sites. The {110} facets appear to be uniformly photoanodic and serve as oxidation sites. When the surfaces are annealed at 1100 °C in

© 2019 WILEY-VCH Verlag GmbH & Co. KGaA, Weinheim

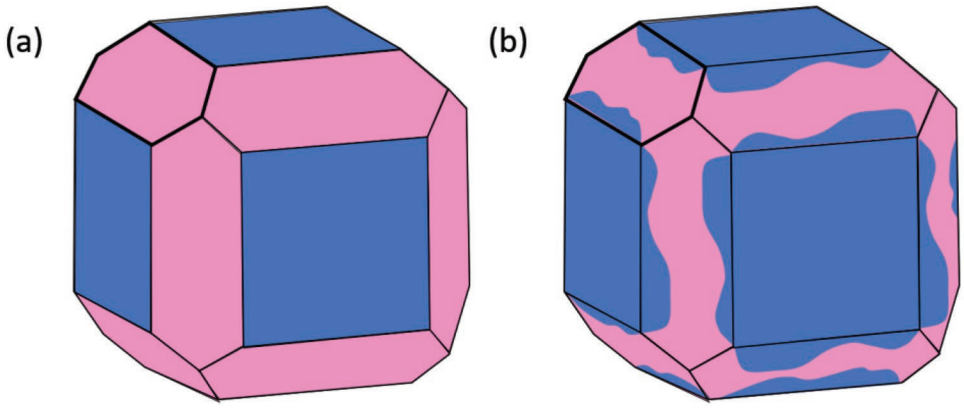

Figure 7. Schematic illustrations of $SrTiO_3$ crystals terminated by {100} and {110} surfaces. a) After the baseline treatment, the {100} surfaces are photocathodic (blue) and the {110} surfaces are photoanodic (pink). b) After annealing at 1100 °C in a Sr-rich environment, portions of the {110} surfaces become photocathodic.

Sr-rich conditions, the {110} surfaces have both photocathodic and photoanodic domains, in contrast to the original faceted surfaces. This demonstrates that thermochemical treatments make it possible to adjust the photocathodic to photoanodic surface area ratio on surfaces of arbitrary orientation.

5. Experimental Section

Polycrystalline $SrTiO_3$ ceramics were prepared from $SrTiO_3$ powder (99.9%, Sigma Aldrich). Disk shaped samples were formed by grinding the as-received powder for 10 min with a mortar and pestle, adding two drops of a polyvinyl alcohol (PVA) solution (5 g PVA per 100 mL water) to ≈1 g of $SrTiO_3$ powder, and pressing the mixture in a half-inch diameter cylindrical die using a table top hydraulic press (Carver). The pressed pellets were then heated according to the following schedule to obtain a dense ceramic with a grain size greater than 5 µm. The samples were heated to 600 °C at 5 °C min^{-1} and held for 1 h, then heated to 1000 °C at 5 °C min^{-1} and held for 8 h, then heated to 1425 °C at 10 °C min^{-1} and held for 6 h, and finally furnace cooled. The dense ceramics were polished with an automated polisher (Buehler AutoMet 250). First, SiC papers with grit sizes of 320, 400, and 600 (Buehler) were used, followed by diamond suspensions (9, 3, 1, and 0.05 µm). Polished samples were then annealed for 8 h at 1250 °C in air. This thermal treatment establishes the initial faceted surface and chemical surface terminations, and is referred to henceforth as the baseline treatment. Subsequent treatments at lower temperatures and of shorter durations do not affect the facet structure formed during the baseline treatment. The samples were then cut into 4 mm × 4 mm square areas (thickness ≈1 mm) using a diamond wire saw. Some samples were subjected to further thermochemical treatments at 1100 °C, with the sample placed in an alumina crucible adjacent to 0.1 g of $Sr_3Ti_2O_7$ for times varying from 1 to 5 h. An attempted procedure using $SrCO_3$ powder as the Sr source was abandoned because it always resulted in the formation of secondary phases on the $SrTiO_3$ surface.

So-called marker reactions that deposit insoluble reaction products at the site of the reaction were used to identify the photocathodic and photoanodic surfaces. For these reactions, a 0.115 M solution of $AgNO_3$, a 0.038 M solution of $Mn(NO_3)_2{\cdot}4H_2O$, and a 0.115 M solution of $Pb(CH_3COO)_2{\cdot}3H_2O$ were used for photoreduction and photooxidation, leading to the photodeposition of solid silver, manganese oxide, and lead oxide, respectively. These reactions have been described elsewhere.[40–42] In this case, an ultraviolet lamp operated at a power of 75 W (photoreduction of Ag^+), 100 W (photooxidation of Mn^{2+}), and 150 W (photooxidation of Pb^{2+}) was used as the illumination source and the exposure times varied from 6 to 75 s. Under these conditions, it is well known that these reactions deposit Ag and MnO_x on $SrTiO_3$ surfaces.[30,33,43,44] The experimental set-up is described in more detail in the Supporting Information. After the photodeposition of reaction products, the surfaces were imaged using a Quanta 200 scanning electron microscope in the SE mode. Images were recorded using a 20 kV beam in low vacuum mode (to prevent charging of the sample) with a spot size number of 5.

Topographic AFM was also used to image the surfaces and to determine the facet orientations in the microscope reference frame. Topographic AFM images were recorded using a Solver-NEXT AFM (NT-MDT) equipped with NC-AFM diamond-like carbon coated tips (Budget Sensors). These images quantify the deviation of the true surface from the average surface plane. The grain orientations were measured by EBSD in a Quanta 600 (FEI) equipped with an OXFORD HKL EBSD system (NordlysNano camera). For each grain of interest, the EBSD measurement returns a set of three Euler angles describing the transformation from the crystal to microscope reference frame. By combining the topographic data measured by AFM with the crystal orientation data measured by EBSD, it is possible to determine the local orientations of the surface facets in the crystal reference frame. To do this, the images were first processed using Gwyddion software[45] and exported in a format that could be read by MATLAB. A MATLAB code was then used to produce a set of vectors representing surface normals in the microscope reference frame. Using the Euler angles measured for that grain, the normals were then transformed to the crystal reference frame and plotted on a standard stereographic projection for visualization and interpretation. Details of this process, as well as the MATLAB codes for visualizing the data and extracting surface normals, are provided in the Supporting Information.

Supporting Information

Supporting Information is available from the Wiley Online Library or from the author.

Acknowledgements

The authors acknowledge the support of National Science Foundation grant DMR 1609369 and use of the Materials Characterization Facility at Carnegie Mellon University supported by grant MCF-677785.

Conflict of Interest

The authors declare no conflict of interest.

© 2019 WILEY-VCH Verlag GmbH & Co. KGaA, Weinheim

Keywords

chemical terminations, facets, photocatalysis, spatial selectivity

Received: April 25, 2019
Revised: May 30, 2019
Published online: July 1, 2019

[1] A. Fujishima, K. Honda, *Nature* **1972**, *238*, 37.
[2] F. Han, V. S. R. Kambala, M. Srinivasan, D. Rajarathnam, R. Naidu, *Appl. Catal., A* **2009**, *359*, 25.
[3] Y. Boyjoo, H. Sun, J. Liu, V. K. Pareek, S. Wang, *Chem. Eng. J.* **2017**, *310*, 537.
[4] A. B. Djurišić, Y. H. Leung, A. M. Ching Ng, *Mater. Horiz.* **2014**, *1*, 400.
[5] S. R. Morrison, *Electrochemistry at Semiconductor and Oxidized Metal Electrodes*, Plenum Press, NY **1980**.
[6] J. J. Glickstein, P. A. Salvador, G. S. Rohrer, *J. Phys. Chem. C* **2016**, *120*, 12673.
[7] J. J. Glickstein, P. A. Salvador, G. S. Rohrer, *J. Mater. Chem. A* **2016**, *4*, 16085.
[8] J. Ran, J. Zhang, J. Yu, M. Jaroniec, S. Zhang Qiao, *Chem. Soc. Rev.* **2014**, *43*, 7787.
[9] J. Yang, D. Wang, H. Han, C. Li, *Acc. Chem. Res.* **2013**, *46*, 1900.
[10] J. Yang, H. Yan, X. Zong, F. Wen, M. Liu, C. Li, *Philos. Trans. R. Soc., A* **2013**, *371*, 20110430.
[11] S. Bai, J. Jiang, Q. Zhang, Y. Xiong, *Chem. Soc. Rev.* **2015**, *44*, 2893.
[12] L. Li, P. A. Salvador, G. S. Rohrer, *Nanoscale* **2014**, *6*, 24.
[13] J. L. Giocondi, G. S. Rohrer, *J. Phys. Chem. B* **2001**, *105*, 8275.
[14] J. L. Giocondi, G. S. Rohrer, *Chem. Mater.* **2001**, *13*, 241.
[15] J. L. Giocondi, G. S. Rohrer, *Top. Catal.* **2008**, *49*, 18.
[16] S. V. Kalinin, D. A. Bonnell, T. Alvarez, X. Lei, Z. Hu, J. H. Ferris, Q. Zhang, S. Dunn, *Nano Lett.* **2002**, *2*, 589.
[17] D. Tiwari, S. Dunn, *J. Mater. Sci.* **2009**, *44*, 5063.
[18] S. Bai, L. Wang, Z. Li, Y. Xiong, *Adv. Sci.* **2017**, *4*, 1600216.
[19] R. Li, F. Zhang, D. Wang, J. Yang, M. Li, J. Zhu, X. Zhou, H. Han, C. Li, *Nat. Commun.* **2013**, *4*, 1432.
[20] Y. P. Xie, G. Liu, L. Yin, H.-M. Cheng, *J. Mater. Chem.* **2012**, *22*, 6746.
[21] R. Munprom, P. A. Salvador, G. S. Rohrer, *Chem. Mater.* **2014**, *26*, 2774.
[22] R. Munprom, P. A. Salvador, G. S. Rohrer, *J. Mater. Chem. A* **2016**, *4*, 2951.
[23] A. S. Pisat, G. S. Rohrer, P. A. Salvador, *Semicond. Sci. Technol.* **2017**, *32*, 103001.
[24] A. S. Pisat, G. S. Rohrer, P. A. Salvador, *J. Mater. Chem. A* **2017**, *5*, 8261.
[25] F. Polo-Garzon, S. Z. Yang, V. Fung, G. S. Foo, E. E. Bickel, M. F. Chisholm, D. E. Jiang, Z. Wu, *Angew. Chem., Int. Ed.* **2017**, *56*, 9820.
[26] Y. Zhu, P. A. Salvador, G. S. Rohrer, *Chem. Mater.* **2016**, *28*, 5155.
[27] Y. Zhu, P. A. Salvador, G. S. Rohrer, *Phys. Chem. Chem. Phys.* **2017**, *19*, 7910.
[28] Y. Goto, T. Hisatomi, Q. Wang, T. Higashi, K. Ishikiriyama, T. Maeda, Y. Sakata, S. Okunaka, H. Tokudome, M. Katayama, S. Akiyama, H. Nishiyama, Y. Inoue, T. Takewaki, T. Setoyama, T. Minegishi, T. Takata, T. Yamada, K. Domen, *Joule* **2018**, *2*, 509.
[29] J. L. Giocondi, P. A. Salvador, G. S. Rohrer, *Top. Catal.* **2007**, *44*, 529.
[30] L. Mu, Y. Zhao, A. Li, S. Wang, Z. Wang, J. Yang, Y. Wang, T. Liu, R. Chen, J. Zhu, F. Fan, R. Li, C. Li, *Energy Environ. Sci.* **2016**, *9*, 2463.
[31] W. Rheinheimer, M. Bäurer, H. Chien, G. S. Rohrer, C. A. Handwerker, J. E. Blendell, M. J. Hoffmann, *Acta Mater.* **2015**, *82*, 32.
[32] T. Sano, D. M. Saylor, G. S. Rohrer, *J. Am. Ceram. Soc.* **2003**, *86*, 1933.
[33] J. L. Giocondi, G. S. Rohrer, *J. Am. Ceram. Soc.* **2003**, *86*, 1182.
[34] N. Erdman, L. D. Marks, *Surf. Sci.* **2003**, *526*, 107.
[35] N. Erdman, O. Warschkow, M. Asta, K. R. Poeppelmeier, D. E. Ellis, L. D. Marks, *J. Am. Ceram. Soc.* **2003**, *125*, 10050.
[36] C. Herring, *Phys. Rev.* **1951**, *82*, 87.
[37] J. W. Cahn, C. A. Handwerker, *Mater. Sci. Eng., A* **1993**, *162*, 83.
[38] R. Bachelet, F. Sánchez, F. J. Palomares, C. Ocal, J. Fontcuberta, *Appl. Phys. Lett.* **2009**, *95*, 141915.
[39] C. Ocal, R. Bachelet, L. Garzo, M. Stengel, F. Sa, *Chem. Mater.* **2012**, *24*, 4177.
[40] J.-M. Herrmann, J. Disdier, P. Pichat, *J. Catal.* **1988**, *113*, 72.
[41] H.-A. Park, S. Liu, Y. Oh, P. A. Salvador, G. S. Rohrer, M. F. Islam, *ACS Nano* **2017**, *11*, 2150.
[42] K. Tanaka, K. Harada, S. Murata, *Sol. Energy* **1986**, *36*, 159.
[43] K. Wenderich, G. Mul, *Chem. Rev.* **2016**, *116*, 14587.
[44] M. Yoshida, T. Yomogida, T. Mineo, K. Nitta, K. Kato, T. Masuda, H. Nitani, H. Abe, S. Takakusagi, T. Uruga, K. Asakura, K. Uosaki, H. Kondoh, *Chem. Commun.* **2013**, *49*, 7848.
[45] D. Nečas, P. Klapetek, *Cent. Eur. J. Phys.* **2012**, *10*, 181.

 © 2019 WILEY-VCH Verlag GmbH & Co. KGaA, Weinheim